Article

Identifying Novel Therapeutics for the Resistant Mutant "F533L" in PBP3 of *Pseudomonas aeruginosa* Using ML Techniques

Tushar Joshi,[⊥] Santhiya Vijayakumar,[⊥] Soumyadip Ghosh, Shalini Mathpal, Sudha Ramaiah,* and Anand Anbarasu*

Read Online

ACCESS | Metrics & More | Article Recommendations | Supporting Information

ABSTRACT: *Pseudomonas aeruginosa* (*P. aeruginosa*) is a highly infectious and antibiotic-resistant bacterium, which causes acute and chronic nosocomial infections. *P. aeruginosa* exhibits multidrug resistance due to the emergence of resistant mutants. The bacterium takes advantage of intrinsic and acquired resistance mechanisms to resist almost every antibiotic. To overcome the drug-resistance problem, there is a need to develop effective drugs against antibiotic-resistant mutants. Therefore, in this study, we selected the F533L mutation in PBP3 (penicillin-binding protein 3) because of its important role in β-lactam recognition. To target this mutation, we screened 147 antibacterial compounds from PubChem through a machine-learning model developed based on the decision stump algorithm with 75.75% accuracy and filtered out 55 compounds. Subsequently, out of 55 compounds, 47 compounds were filtered based on their drug-like activity. These 47 compounds were subjected to virtual screening to obtain binding affinity compounds. The binding affinity range of all 47 compounds was −11.3 to −4.6 kcal mol^{-1}. The top 10 compounds were examined according to their binding with the mutation point. A molecular dynamic simulation of the top 8 compounds was conducted to understand the stability of the compounds containing the mutated PBP3. Out of 8 compounds, 3 compounds, namely, macozinone, antibacterial agent 71, and antibacterial agent 123, showed good stability and were validated by RMSD, RMSF, and binding-free analysis. The findings of this study revealed promising antibacterial compounds against the F533L mutant PBP3. Furthermore, developments in these compounds may pave the way for novel therapeutic interventions.
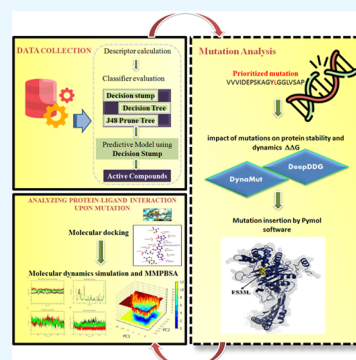
1. INTRODUCTION

Pseudomonas aeruginosa (*P. aeruginosa*) is a gram-negative, rod-shaped, aerobic opportunistic bacterial pathogen. This bacterium plays an important role in nosocomial infections, especially in individuals with weakened host defenses.[1,2] *P. aeruginosa* also appears to be the third most common cause of urinary tract infection and the second most common cause of pneumonia.[3,4] Currently, *P. aeruginosa* infections are treated primarily with eight classes of antibiotics: aminoglycosides (tobramycin, gentamicin, netilmicin, and amikacin), cephalosporins (ceftazidime and cefepime), carbapenems (imipenem and Meropenem), fluoroquinolones (ciprofloxacin and levofloxacin), monobactams (aztreonam), fosfomycin and polymyxins (colistin and polymyxin B), and penicillins with β-lactamase inhibitors (BLIs) (ticarcillin and piperacillin in combination with clavulanic acid or tazobactam).[5] Despite these treatments, multidrug-resistant (MDR) *P. aeruginosa* bacteria remain a significant problem for hospitals.[6] Due to its resistance to various drugs, comprising third-generation cephalosporins and carbapenems, the World Health Organization (WHO) lists it as one of the most important priority pathogens.

The rise of MDR *P. aeruginosa* isolates has become a global public health concern. Infection with these isolates limits available treatments and increases morbidity and mortality.[7] Carbapenems represent an important therapeutic option for the management of gram-negative bacteria. However, the increase in carbapenem resistance of *P. aeruginosa* raises serious concerns, especially for patients who are in critical condition. Consequently, *P. aeruginosa* is now considered an emergency pathogen by the WHO, meaning that novel treatment strategies are desperately needed.[8] As per the report from WHO, if no intervention is taken to address antimicrobial resistance (AMR), by the year 2050, the world could face 10 million deaths annually and could experience a global economic crisis as severe as the crisis of 2008−2009.[9] According to a 2019 study, AMR infections accounted for about 4.95 million deaths, with 1.27 million directly linked to drug resistance. The study also highlights AMR as the greatest threat to populations in South Asia and sub-Saharan Africa compared to all other countries studied.[10] In addition to

developing resistance, *P. aeruginosa* is also able to acquire antibiotic tolerance through the production of complex bacterial clusters known as biofilms, which stick to surfaces and are encased in a self-produced matrix, preventing them from being exposed to antibacterial agents. Biofilm-forming bacterial pathogens are more resistant to antibiotics; strains of *P. aeruginosa* that can form biofilms are 20−30% resistant to fluoroquinolones and 12−22% resistant to gentamicin.[11] In addition to biofilm formation, *P. aeruginosa* exhibits several drug-resistance mechanisms for survival. These include modifications to porins embedded in the outer membrane, which limit the permeability of antibiotics; the degradation of β-lactams by β-lactamases; modifications in protein targets, especially penicillin-binding proteins (PBPs) that reduce the efficiency of drug binding; and increased activity in pumping out antibiotics from cells through efflux pumps.[12,13]

In this study, we selected PBP3 for this investigation because, in addition to being crucial to the bacterium's survival, it is a prime target for the creation of antibacterial drugs. This target is clinically validated, and the absence of a human counterpart makes it less likely to cause drug interactions. Since the catalytic domain of PBP3 is located in the periplasm, potential small molecule inhibitors can reach it.[14] Usually, β-lactam antibiotics target the PBP3. However, the potency of β-lactams has significantly changed with the emergence and spread of MDR strains, including genetically or plasmid-encoded β-lactamases and additional resistance mechanisms (e.g., efflux transporters and target mutations). β-lactamases destroy the β-lactam antibiotics' antibacterial activity by hydrolyzing the β-lactam ring.[14]

The most prevalent PBP3 variations that could impact β-lactam activity are substitutions of amino acids, primarily localized near the active site, specifically the catalytic Ser-XX-Lys motif.[13] Among all of the mutations on the motif, mutant F533L (533L) has been demonstrated to play an important role in β-lactam recognition. Due to mutation at the 533L position of PBP3, it reduces the affinity for meropenem antibiotics.[15]

Thus, under the current circumstances, there is a great need to find effective antibacterial drugs to treat mutation effectively. Since the synthesis of new drugs is extremely difficult, we performed an *in-silico* analysis of antibacterial compounds from PubChem against the *P. aeruginosa* enzyme PBP3. We hope that the findings of this study can help in the search for new drug compounds against *P. aeruginosa*.

2. RESULTS

2.1. Mutation Stability Analysis. Both DynaMut2 and DeepDDG predicted the mutation 533L to destabilize the overall protein structure with −0.94 and −0.097 kcal/mol $\Delta\Delta G$ values, respectively (Table 1). The destabilizing effect of the mutation can be seen through intermolecular interactions where there was a slight loss in the number of interactions (hydrophobic and polar) in the mutant structure compared to the wild-type. It was also observed that the mutant structure

Table 1. Destabilizing Value of Mutation Position Using DynaMut2 and DeepDDG Server

predictors	F533L
DynaMut2 $\Delta\Delta G$ (kcal/mol)	−0.94 kcal/mol (destabilizing)
DeepDDG $\Delta\Delta G$ (kcal/mol)	−0.097 kcal/mol (destabilizing)

had one van der Waals interaction with Thr487 while it was absent in the wild-type structure (Table 2) (Figure 1).

Table 2. Different Types of Interaction Observed in Wild-Type and Mutant Structures of PBP3 Using DynaMut2 Server

type of interaction	wild-type (PHE533)	interacting residues	mutant (LEU533)	interacting residues
clash	3	LEU536, GLY535, VAL537	1	VAL537
van der Waals	0		1	THR487
hydrogen	4	LEU536, VAL537, THR487	4	LEU536, VAL537, THR487
hydrophobic	3	LEU536, VAL333	2	LEU536, THR487
polar	6	LEU536, VAL537, THR487, GLY535	5	LEU536, VAL537, THR487

2.2. Performance of Machine-Learning (ML) Classifier and Data Set Screening. To create the best ML model for distinguishing between antibacterial substances and non-antibacterial substances, we constructed classification models using ML approaches. Several statistical metrics, as indicated in Table 3, were used to assess the models' performance. Using 10-fold cross-validation (CV) on the training data set, a collection of models was trained using three distinct classification algorithms: decision stump, decision table, and J48. All of the classifiers that were utilized are compiled in Table 3 based on the performance index. When evaluating the model, the kappa statistic's value represents the degree of consistency between the real and model classes, and a value of 1 denotes perfect agreement between the ground truth and the classifier model's classification in that instance. In comparison to the other models, the decision stump model displayed the highest kappa statistic value of 0.5, indicating a moderate level of agreement and the final root mean square error (RMSE) value of 0.42. The decision stump was shown to be the best classifier overall, followed by the decision table and J48, according to the analysis. The decision stump, decision table, and J48 had accuracy rates of 75.75, 72.72, and 69.69%, in that order. The classifier's accuracy in properly recognizing positively and negatively labeled occurrences was evaluated using sensitivity and specificity plots, which were used to determine the optimal models for each data set (Figure 2). Decision stump was the most sensitive classifier for the data set, and the decision table was the least sensitive. The specificity of decision stump ranged from 53 to 60%, and the sensitivity ranged from 78 to 89%. Furthermore, additional performance metrics such as receiver operating characteristic (ROC) curve analysis were employed to demonstrate the flexibility of the model. The performance of the binary classifier model when its discrimination threshold is changed is displayed by the ROC curve. The ROC curve of the current model initially showed a strong relationship with the true positive rate axis, which represents maximizing the sensitivity and minimizing false positive rates (maximizing the specificity and sensitivity). The ROC value of the decision table was 0.77, that of the decision stump was 0.76, and that of J48 was 0.73. Ultimately, the top model decision stump was selected for virtual screening based on its performance. The model indicated that 55 of the 147 antibacterial compounds were
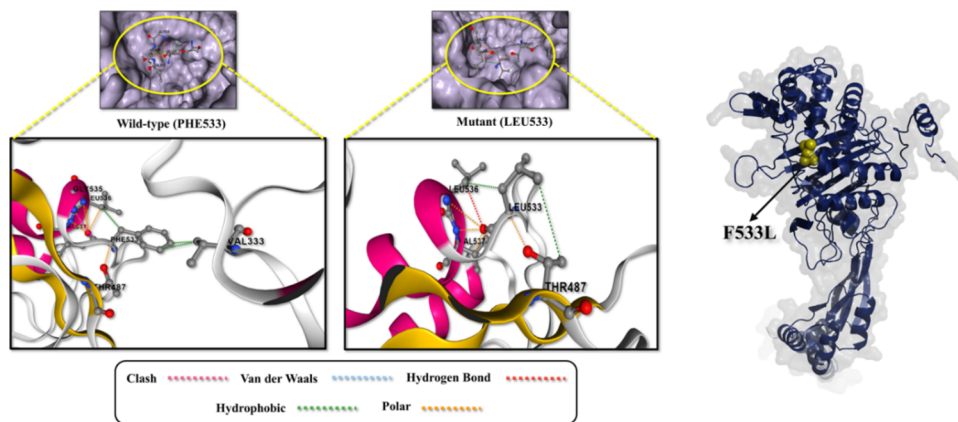
Figure 1. 3D interactive visualization of bonds formed between neighboring amino acid residues of wild-type and mutant-type proteins penicillin-binding protein 3. The figure also depicted mutation point "F533L" (brown color) on PBP3 protein.

Table 3. Comparison of Performance of Different Classifiers for the Development of the Screening Model in the Training Set

classifier name	correctly classified instances % (value)	kappa statistic	mean absolute error	root mean square error	MCC	ROC area
decision stump	75	0.5	0.27	0.42	0.51	0.76
decision table	72	0.37	0.32	0.42	0.37	0.77
J48	69	0.34	0.29	0.51	0.35	0.73

active and 92 molecules were inactive. Finally, 55 active compounds were considered for further research.

2.3. Drug Likeness Activity. The properties of drug likeness of the 55 compounds from the library were analyzed and are shown in Supplementary Table S1. The DruLiTo software is used to determine the various properties of the ligand such as molecular weight, logP, H bond donors, and H bond acceptors of ligands. Out of 55 compounds, 47 were followed Lipinski's five rules. All 47 compounds have molecular weights less than 500 Da (Da), LogP values less than 5, the number of hydrogen bond acceptors is less than 10, and the number of hydrogen bond donors is less than five compounds. It was shown that these chemicals follow Lipinski's five rules (Table 4). After screening, these 47 compounds were employed in molecular docking.

2.4. Molecular Docking. To find the potential inhibitors from the docked compounds with the mutation site of the PBP3 receptor, we determined the ligands' docked poses with the mutation position of PBP3 at the 533L amino acid position. After the top 10 best-docked conformers with the highest affinity for the PBP3 receptor were selected, the binding mechanism and molecular interactions in the PBP3 mutant region were examined. Furthermore, those compounds that showed binding to the mutation point at the 533L positions of PBP3 are considered preferential in docking analysis. The findings of the interaction analysis show that all top 10 compounds, namely, antibacterial agent 113, antibacterial agent 30, antibacterial agent 71, macozinone, antibacterial agent 123, antibacterial agent 82, antibacterial agent 53, sparfloxacin, pretomanid, and antibacterial agent 31 showed hydrophobic interactions with 533L amino acid (Figure 3). The antibacterial agent 113 forms one hydrogen bond Y409 and 14 hydrophobic bonds N351, Y407, S294, T487, S349, S485, G534, G535, K348, I347, S334, 533L, V333, and R489 with −11.3 kcal mol^{-1} binding energy (Figure 3A). The antibacterial agent 30 forms three hydrogen bonds Y407, N351, and S485 and nine hydrophobic bonds R489, Y409, V333, S349, G486, G535, 533L, T487, and Y498 and showed −10.4 kcal mol^{-1} binding energy (Figure 3B). The antibacterial agent 71 showed −10.4 kcal mol^{-1} binding energy and form two hydrogen bonds S485 and N351 and seven hydrophobic bonds 533L, V333, Y409, R331, Y498, T487, and S349 (Figure 3C). Macozinone showed −10.3 kcal mol^{-1}
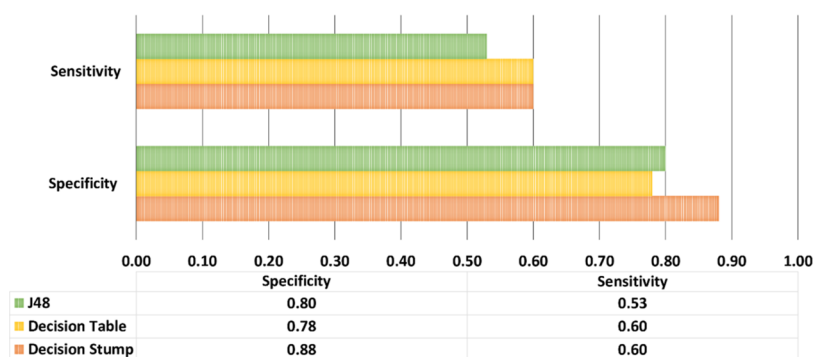

Figure 2. Statistical performance of various classifiers used for screening test sets of machine-learning modeling.

Table 4. Drug Likeness Properties of the Top 10 Docked Compounds with PBP3

ligands	PubChem-ID	MW (g/mol)	logP	HBA	HBD
antibacterial agent 113	164517170	487.12	2.243	6	1
antibacterial agent 30	156783454	463.16	2.624	6	2
antibacterial agent 71	163196389	468.21	1.903	5	1
macozinone	57331386	456.14	4.486	4	0
antibacterial agent 123	165413023	441.05	3.32	4	2
antibacterial agent 82	163196417	342.14	4.655	4	2
antibacterial agent 53	163323821	395.09	−1.132	9	2
sparfloxacin	60464	392.17	2.353	7	3
pretomanid	456199	359.07	2.636	5	0
antibacterial agent 31	163323786	345.99	3.216	5	0
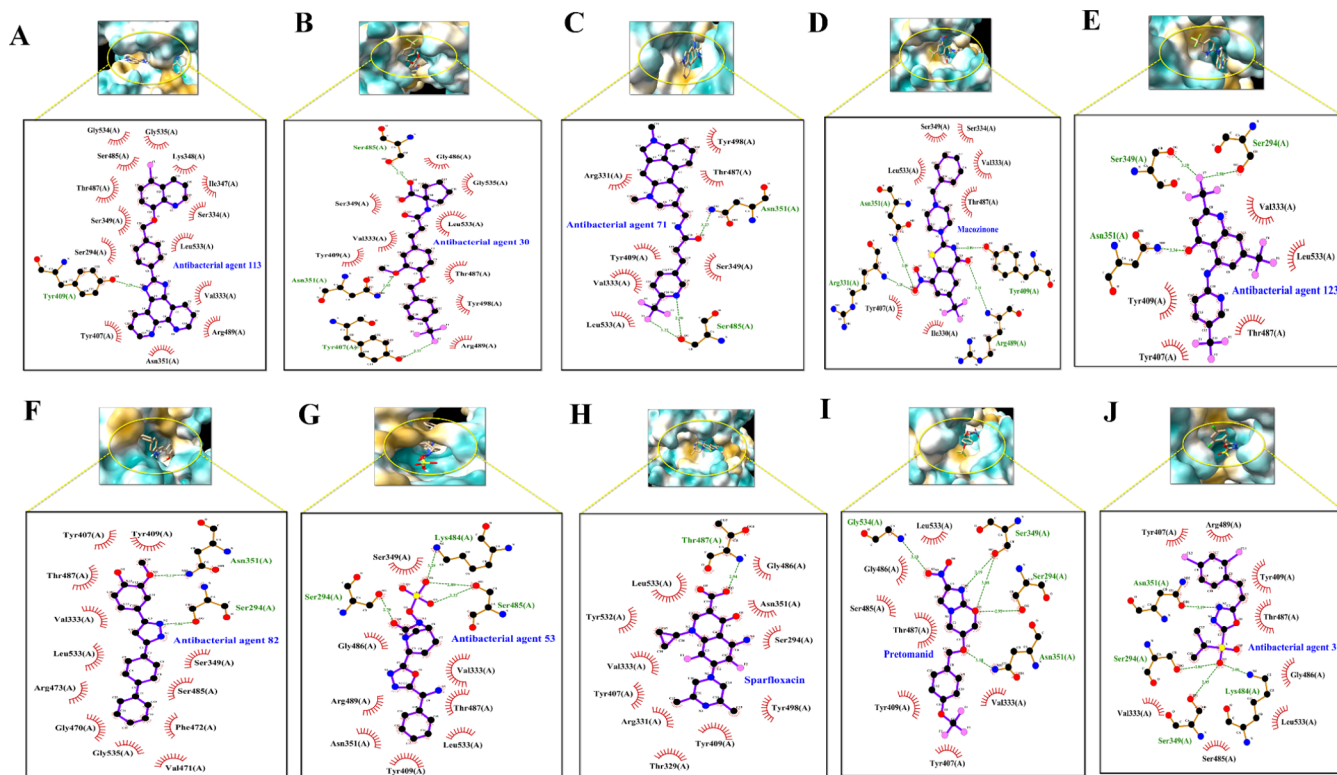
Figure 3. 2D and 3D interaction of 10 compounds, namely, (A) antibacterial agent 113, (B) antibacterial agent 30, (C) antibacterial agent 71, (D) macozinone, (E) antibacterial agent 123, (F) antibacterial agent 82, (G) antibacterial agent 53, (H) sparfloxacin, (I) pretomanid, and (J) antibacterial agent 31 with mutated position 533L amino acid (hydrophobic interaction) and with transpeptidase domain of PBP3.

binding energy and form four hydrogen bonds R489, Y409, R331, and N351 and seven hydrophobic bonds I330, Y407, 533L, S349, S334, V333, and T487 (Figure 3D). The antibacterial agent 123 showed −10.1 kcal mol^{-1} binding energy and form three hydrogen bonds N351, S349, and S294 and five hydrophobic bonds Y409, Y407, 533L, V333, and T487 (Figure 3E). The antibacterial agent 82 forms two hydrogen bonds N351 and S294 and 12 hydrophobic bonds V471, G535, G470, R473, 533L, V333, T487, Y407, Y409, S485, S349, and F472 with −9.6 kcal mol^{-1} binding energy (Figure 3F). The antibacterial agent 53 forms four hydrogen bonds (K484, S294 and two H bonds with S485) and eight hydrophobic bonds G486, R489, N351, Y409, 533L, T487, V333, and S349 with −9.4 kcal mol^{-1} binding energy (Figure 3G). The sparfloxacin showed −9.1 kcal mol^{-1} binding energy and form one hydrogen bond Thr487 and 11 hydrophobic bonds 533L, Y532, V333, Y407, R331, T329, Y409, Y498, S294, N351, and G486 (Figure 3H). The pretomanid forms

five hydrogen bonds (G534, S294, N351 and two H bonds with S349) and seven hydrophobic bonds Y407, Y409, T487, S485, G486, 533L, and V333 with −9.1 kcal mol^{-1} binding energy (Figure 3I) and the antibacterial agent 31 showed −9.1 kcal mol^{-1} binding energy and showed four hydrogen bonds S349, K484, S294, and N351 and eight hydrophobic bonds V333, S485, 533L, G486, T487, Y409, R489, and Y407 (Figure 3J) (Table 5).

2.5. Absorption, Distribution, Metabolism, Excretion, and Toxicity (ADMET) Properties. The results of ADMET are shown in Table 6. All of the selected compounds showed a very good possibility of being absorbed in the human intestine with human intestinal absorption (HIA) properties. Also, all compounds showed a very good possibility of crossing the blood−brain barrier (BBB+) except antibacterial agent 53 and sparfloxacin. Apart from these properties, we have checked carcinogenic properties, and all compounds showed non-carcinogenicity properties, an important pharmacokinetic

Table 5. Binding Energy of the Top 10 Screened Compounds against PBP3

ligands	PubChem-ID	binding energy
antibacterial agent 113	164517170	−11.3
antibacterial agent 30	156783454	−10.4
antibacterial agent 71	163196389	−10.4
macozinone	57331386	−10.3
antibacterial agent 123	165413023	−10.1
antibacterial agent 82	163196417	−9.6
antibacterial agent 53	163323821	−9.4
sparfloxacin	60464	−9.1
pretomanid	456199	−9.1
antibacterial agent 31	163323786	−9.1

Table 6. ADMET Properties of the Screened Compounds

ligands	carcinogens	blood–brain barrier	human intestinal absorption
antibacterial agent 113	noncarcinogens	BBB+	HIA+
antibacterial agent 30	noncarcinogens	BBB+	HIA+
antibacterial agent 71	noncarcinogens	BBB+	HIA+
macozinone	noncarcinogens	BBB+	HIA+
antibacterial agent 123	noncarcinogens	BBB+	HIA+
antibacterial agent 82	noncarcinogens	BBB+	HIA+
antibacterial agent 53	noncarcinogens	BBB −	HIA+
sparfloxacin	noncarcinogens	BBB −	HIA+
pretomanid	noncarcinogens	BBB+	HIA+
antibacterial agent 31	noncarcinogens	BBB+	HIA+

property in drug discovery. All of these properties indicate that all of the selected compounds have good ADMET properties.

2.6. Molecular Dynamic (MD) Simulation. Further to assess the flexibility, structural behavior, and stability of the top eight highly active docked molecules, a 100 ns MD simulation was calculated. MD simulations reveal insight into the compounds' dynamic behavior, and this dynamic behavior is used to obtain the information that can be used in drug discovery. The top eight protein−ligand complexes were simulated. MD simulations were also performed on the PBP3 wild-type and mutant proteins without ligands to compare the results. To verify the protein's conformational stability, additional parameters such as the interaction energy, radius of gyration (Rg), root-mean-square deviation (RMSD), and root-mean-square fluctuations (RMSF) of residues are also evaluated for each system. After RMSD analysis, out of the eight compounds, three compounds, namely, macozinone, antibacterial agent 71, and antibacterial agent 123, showed promising inhibitory activity against the PBP3. Therefore, only these three compounds were further subjected to additional analysis and description.

2.6.1. Root Mean Square Deviation. The RMSD is an important parameter to analyze the equilibrium in the MD trajectory, which is estimated for the backbone atoms of PBP3 and the protein−ligand complex. Both the wild-type and mutant showed good stability in terms of only a single protein. The RMSD value of the wild-type is 0.21 ± 0.26 nm, and the RMSD value of the mutated type is 0.312 ± 0.03 nm. In the case of complexes, all complexes showed fluctuations up to 10 ns, after which all showed stability with PBP3 (Figure 4A). In the case of the PBP3 and macozinone ligand complexes, the RMSD value was calculated as 0.62 ± 0.101 nm. The fluctuations had dropped to about 0.2 to 0.3 ns around the

30 ns period. A clear and noticeable 0.5 nm deviation was observed in the residuals of the RMSD values with an increase in time from 45 to 55 ns. Most of the residues showed stable states during the 100 ns simulation. At the same time, the PBP3 and antibacterial agent 71 ligand complex showed fluctuations by about 0.3 nm from 25 to 27 ns and remained stable with an RMSD value of 1.05 ± 0.151 nm until the end of the simulation. In contrast, in the case of PBP3 and the antibacterial agent 123 ligand complexes, the RMSD value showed 0.94 ± 0.065. Most of the residues of this complex showed a steady state during the 100 ns simulation (Figure 5A).

2.6.2. Root Mean Square Fluctuation. The calculation of the RMSF shows the variation of the complex with time against each residue. We have demonstrated only PBP3 (wild-type and mutant) and complex compounds during 100 ns simulations. In this study, mainly we have focused on the mutation point site at the 533L positions. In the case of both wild-type and mutant proteins at the position of 533, the fluctuation is low. In the other position, the residue fluctuation is high in the case of mutated protein, which is 0.2 to 0.5 nm as compared to the wild-type structure (Figure 4B). The low fluctuation in the position of 533 shows that, due to mutation, the protein has not lost its stability. In the case of ligand complexes, the overall fluctuation in all complexes is very low except for some residues, i.e., around 100 and 200 position residues during 100 ns simulations. This means that after making a complex with ligands, the protein does not have its stability at the mutation point. The fluctuation shown in Figure 5B clearly shows that it is more than 0.4 to 0.6 nm in all complexes.

2.6.3. Radius of Gyration. Rg values are calculated throughout to understand the compactness, stability, and folding of the protein structure. The structural density of PBP3 and its complexes was assessed by analyzing their Rg values. The Rg values of wild-type, mutated protein, and all three protein complexes were consistent with each other. In the case of only the protein structure of the wild-type, it showed fewer deviations with a value of 2.531 ± 0.124 nm compared to the mutated structure. The mutated protein structure showed a 0.1 nm deviation with 2.429 ± 0.127 nm (Figure 4C). In the case of all complexes, the Rg value of macozinone is 2.523 ± 0.199 nm, antibacterial agent 71 is 2.528 ± 0.244 nm, and antibacterial agent 123 is 2.552 ± 0.236 nm (Figure 5C). The Rg value of only protein and ligand complexes are the same, and it shows that the compactness of protein is not changing after binding the ligand. Finally, the Rg results indicate that all complexes exhibit a good compact structure.

2.6.4. Interaction Energy (Van Der Waals). The average Lennard-Jones Short Range (LJ-SR) interaction (van der Waals) calculation was performed by using the Parrinello−Rahman parameter of GROMACS to estimate the LJ-SR interaction energies associated with the PBP3-ligand complexes. Every complex's average LJ-SR interaction (van der Waals) was found to be within the permissible range. The interaction energy of complexes macozinone was −108.243 kJ/mol, antibacterial agent 71 was −143.548 kJ/mol, and antibacterial agent 123 was −113.605 kJ/mol (Figure 5D). The LJ-SR interaction energy indicated the highest binding affinity with PBP3 and demonstrated that the investigated compounds could bind favorably with PBP3.

2.6.5. Hydrogen Bond. Hydrogen bonding is one of the most crucial interactions for stabilizing protein−ligand
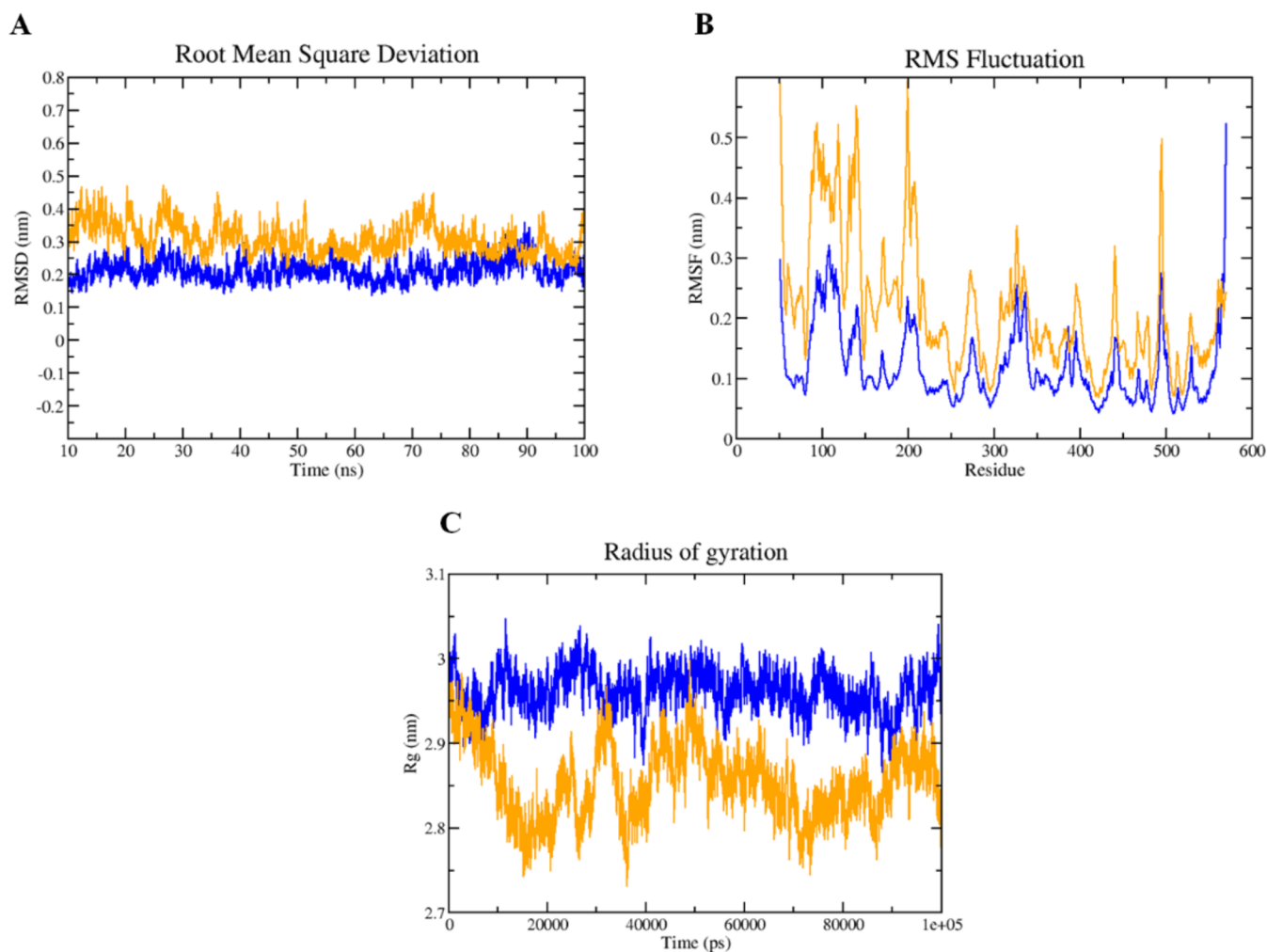
Figure 4. Wild-type and mutant protein stability analysis during 100 ns molecular dynamics simulation (wild-type PBP3 (blue) and mutant PBP3 (orange)). (A) Root mean square deviation, (B) root mean square fluctuation, and (C) radius of gyration

complexes. The number of hydrogen bonds formed in the PBP3-ligand complex during the 100 ns trajectory is depicted in Figure 6A. Macozinone shows the maximum number of hydrogen bonds followed by antibacterial agent 123 and antibacterial agent 71 with 4, 3, and 2, respectively. The analysis revealed that in all compounds, the hydrogen bonds between the protein and ligand complexes remained intact throughout the 100 ns simulation (Figure 6A). Therefore, hydrogen bonds play a specific role and contribute significantly to the binding energy of all complexes.

2.6.6. Principal Component Analysis (PCA). The initial few eigenvectors, which are crucial for the overall mobility of the protein during the MD simulation of the PBP3-macozinone, PBP3-antibacterial agent 71, and PBP3-antibacterial agent 123 complexes, were calculated using PCA analysis. Forty eigenvectors were chosen for this investigation to compute coordinated motions. For every protein−ligand complex, the motion of the eigenvector is shown in Figure 6B. The first ten eigenvectors account for 81.84, 77.63, and 77.96% of the motions in the 100 ns simulation period for PBP3-macozinone, PBP3-antibacterial agent 71, and PBP3-antibacterial agent 123, respectively.

The eigenvalues of PBP3-macozinone, PBP3-antibacterial agent 71, and PBP3-antibacterial agent 123 complexes are 19, 11.4, and 12 nm^2, respectively. These values were obtained by

diagonalizing the covariance matrix of atomic fluctuations in decreasing order versus the corresponding eigenvector for all complexes (Figure 6B).

Furthermore, a 2D projection plot was created using PCA to investigate the dynamics of the protein−ligand complex. As a result, for motion analysis, we first employed two PCs, PC1 and PC2. The hit compounds PBP3-macozinone, PBP3-antibacterial agent 71, and PBP3-antibacterial agent 123 are represented by the projection of two eigenvectors in Figure 6C. In the 2D projection plot, the complex taking up less phase space represents the stable cluster, while the complex taking up more space represents the nonstable cluster. The layout revealed that each complex took up the same area (Figure 6C). As a result, each chemical compound is stable and has the potential for use in drug development.

The Gibbs energy landscape was examined by using the projection of their first principal component (PC1) and second (PC2) eigenvectors (Figure 7A−C). In all three protein−ligand complexes, the global energy minima states were displayed by Gibbs free energy landscapes, indicating the energetically favored protein configurations. Energetically unfavorable protein configurations were depicted in red in the 2D projection, whereas the minimum energy conformations of proteins with maximum stability were shown in dark blue. The range of Gibbs energy values is 11.5, 12, and 12.54
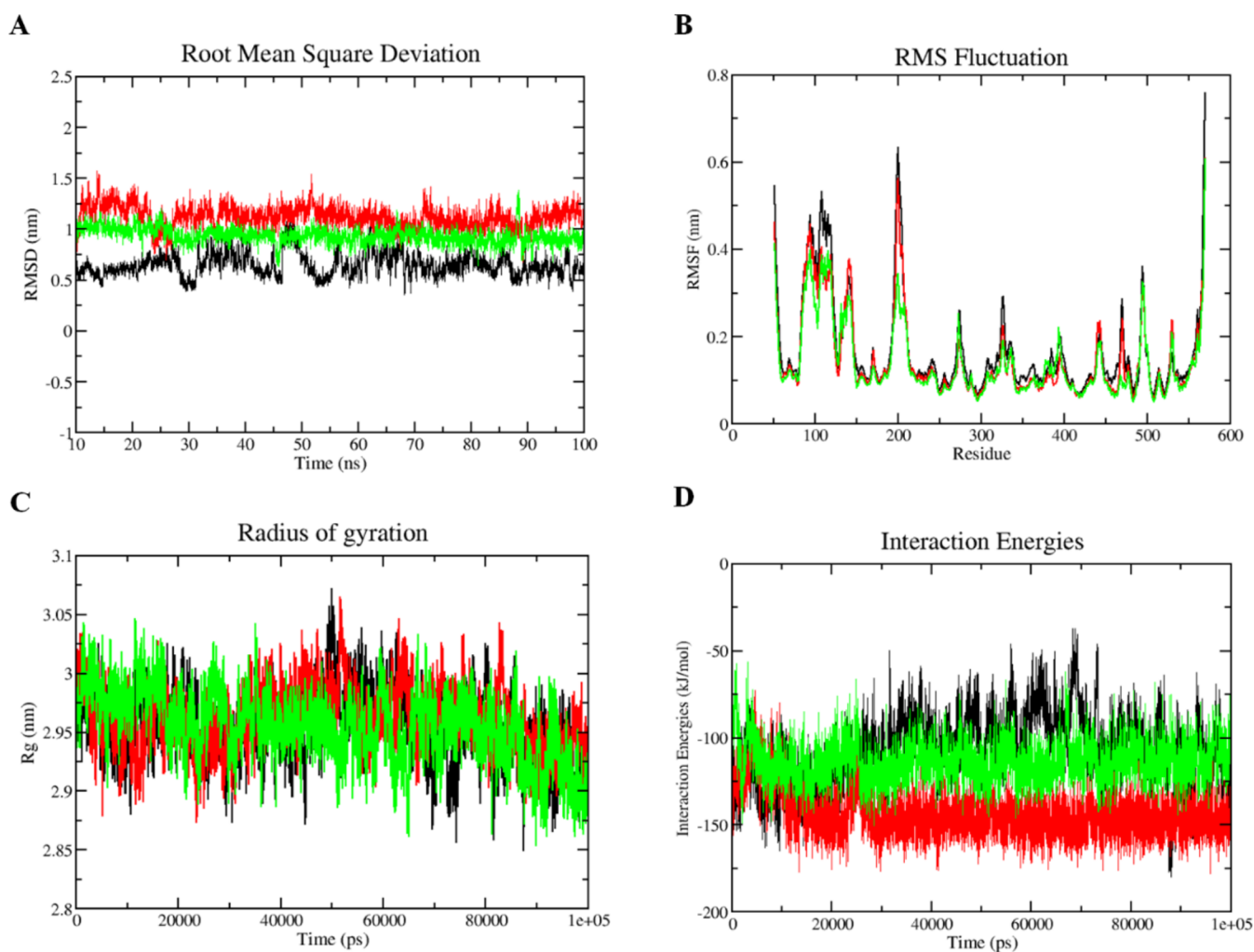
Figure 5. Binding stability analysis of the screened compounds with PBP3 during 100 ns molecular dynamics simulation (PBP3-macozinone (black), PBP3-antibacterial agent 71 (red), and PBP3-antibacterial agent 123 (green)). (A) Root mean square deviation, (B) root mean square fluctuation, (C) radius of gyration, and (D) interaction energy.
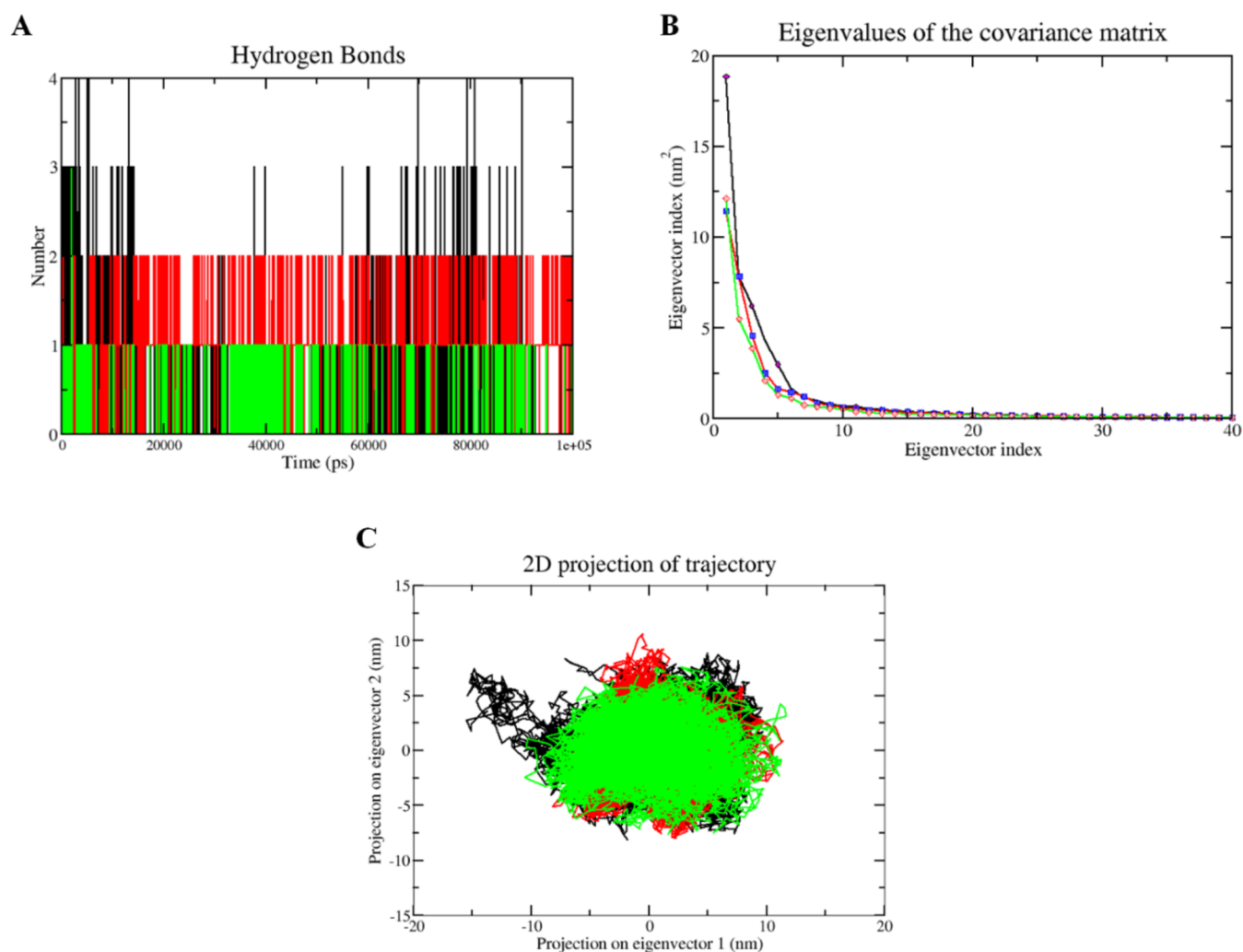
kJ/mol, respectively (Figure 7). The Gibbs free energy landscape analyzes the path of fluctuation in the two structures for all Cα atoms of the free PBP3-macozinone, PBP3-antibacterial agent 71, and PBP3-antibacterial agent 123 complex. The conformational stability states that all of the three compounds with PBP3 were well represented by PCA analysis.

2.6.7. Binding Energy. The gmx_MMPBSA test tool was applied to determine the total binding-free energy of the three hits with PBP3. The MM/GBSA energy components were analyzed, and graphs were created using the gmx_MMPBSA_ana visualization tools. All three complexes had the MMPBSA run for 100 ns (Table 7). Figure 8 displays bar charts that show the energy values for the summed components ($\Delta GGAS$, $\Delta GSOLV$, and $\Delta GTOTAL$) and individual components (ΔEEL and $\Delta EVDWAALS$). Additionally, Figure 8 also depicts the value of $\Delta GGAS$ and $\Delta GSOLV$ for each of the three compounds, which includes $\Delta EVDWAALS$, ΔEEL, ΔEGB, and $\Delta ESURF$ values. The lowest values of $\Delta GTOTAL$ binding-free energy were reported for all complexes: PBP3-macozinone, PBP3-antibacterial agent 71, and PBP3-antibacterial agent 123, with values of −19.19, −27.5, and −19.23 kcal/mol, respectively (Figure 8).

2.7. Molecular Property Functions analysis. Three known antibacterial compounds cefepime, ciprofloxacin, and ampicillin along with the three screened compounds macozinone, antibacterial agent 71, and antibacterial agent 123 were subjected to analysis of their molecular properties. It has been identified that atom counts, functional group counts, and ring counts were similar in both known antibacterial compounds and the screened compounds. In the finalized screened compounds, the atoms identified were carbon, fluorine, hydrogen, nitrogen, oxygen, and sulfur; the functional groups were secondary amines (R_2NH), tertiary amines (R_3N), and carbonyl group (RCOR). In addition to atoms and functional groups, the rings and aromatics were also found in all three screened compounds, similar to that of known antibacterial compounds. This indicates that these screened compounds can be used against *P. aeruginosa* (Figure 9).

3. DISCUSSION

Infections caused by MDR *P. aeruginosa* are one of the leading threats to the global AMR burden and a major cause of morbidity and mortality. The epidemiology and mechanisms of resistance of *P. aeruginosa* are constantly changing, which has an important impact on existing and newly developing β-lactam antibiotics.[16] At present, β-lactam antibiotics are and

A

Hydrogen Bonds

B

Eigenvalues of the covariance matrix

C

2D projection of trajectory

Figure 6. (A) Hydrogen bond, (B) eigenvalues plot vs first 40 eigenvectors, and (C) protein motion phase space of all the protein−ligand complexes. The color code for all panels is PBP3-macozinone (black), PBP3-antibacterial agent 71 (red), and PBP3-antibacterial agent 123 (green).

will remain an important treatment option for *P. aeruginosa* infections. However, treatment becomes more challenging as more dangerous MDR bacterial strains emerge. R504C/H and 533L are the most frequently reported mutations within the protein domains linked to the creation and maintenance of the inactivating complex β-lactam-PBP3.[17] Clinical isolates of *P. aeruginosa* that have acquired resistance to one of the last lines of defense "the carbapenems" remain a serious problem.[18] These particular mutations have been shown to emerge in vivo during chronic respiratory infections in patients with cystic fibrosis (CF)[19,20] as well as in vitro upon exposure to meropenem,[15] aztreonam,[21] and ceftazidime.[22] In one study, it was found that 533L and R504C mutations were found in the PBP3 that exposure to meropenem during in vitro evolution studies and among CF patients treated with this drug.[23] A different investigation found that the sequence variation 533L showed a lower affinity against meropenem but not against ceftazidime.[15]

Therefore, this study addresses an important issue of antibiotic resistance in *P. aeruginosa* by focusing on the 533L mutation in PBP3, which is a key enzyme in bacterial survival, and we explored the potential therapeutics against the emerging mutation 533L in the PBP3 by using combined

advanced computational techniques. Various studies have found where researchers have targeted the PBP3. According to data from the Clark et al. 2019 study, PBP3 is a common adaptive target that may aid in the evolution of β-lactam resistance of *P. aeruginosa*.[23] In another study by Sahare and Moon, they targeted the transpeptidase (TP) domain of PBP3 of *E. coli*.[24] The TP domain is a site that is responsible for the penicillin-binding. 533L mutation is also present in the TP domain of PBP3 and key position for antibiotic recognition. In the study of Glen and Lamont 2021, they have clearly shown that a position of "F533" is present in the TP domain of the PBP3, and mutation at this point reduces the efficiency of meropenem binding.[13,25] β-lactam derivatives have effectively targeted the TP domain site; however, due to their extensive usage, resistant bacterial strains have emerged, which utilize several strategies to evade the antibiotics' deadly effects.[26]

In this study, we used antibacterial agents from PubChem. We checked these compounds for their binding and affinity toward PBP3 of *P. aeruginosa*. Fifty-five antibacterial compounds were screened using virtual screening through machine learning followed by screening for drug-like properties. Among them, 47 compounds were found to follow Lipinski's rule. The rule is used to evaluate the medicinal or
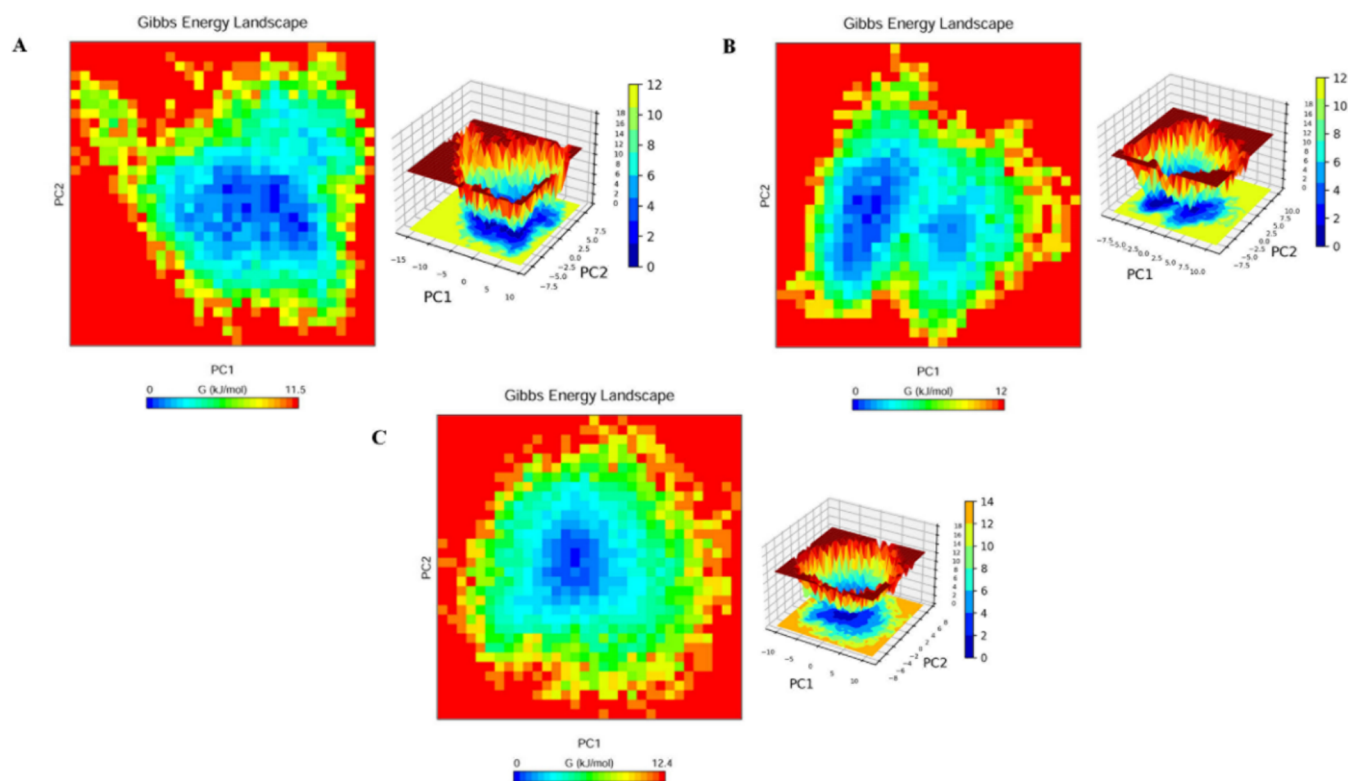
Figure 7. 2D and 3D Gibbs free energy landscapes of compounds. (A) PBP3-macozinone, (B) PBP3-antibacterial agent 71, and (C) PBP3-antibacterial agent 123.

Table 7. Binding-Free Energy Calculations of Protein and Ligand Complex Using the gmx_MMPBSA Method[a]

ligands	VDWAALS	EEL	EGB	ESURF	GGAS	GSOLV	TOTAL
macozinone	−29.03 ± 5.29	−2.48 ± 4.1	16.53 ± 3.95	−4.21 ± 0.71	−31.51 ± 7.04	12.32 ± 3.63	−19.19 ± 4.98
antibacterial agent 71	−37.53 ± 3.17	−4.79 ± 3.48	19.48 ± 3.0	−4.66 ± 0.33	−42.31 ± 4.71	14.81 ± 2.99	−27.5 ± 4.79
antibacterial agent 123	−29.99 ± 2.9	−1.19 ± 2.92	16.61 ± 3.27	−4.66 ± 0.35	−31.18 ± 4.49	11.95 ± 3.1	−19.23 ± 2.66

[a]ΔVDWAALS: van der Waals molecular mechanics energy; ΔEEL: electrostatic molecular mechanics energy; ΔEGB: polar contribution to the solvation energy; ΔGGAS: total gas phase molecular mechanics energy; ΔESURF: solvent accessible surface area; ΔGSOLV: total solvation energy; ΔGTOTAL: total relative binding energy.

biological activities of chemical compounds that can potentially make the compound an orally active drug for humans. The five rule of Lipinski states that the molecular weight of any compound should be under 500 Da, the LogP value should be under 5, the number of hydrogen bond acceptors should be under 10, and the hydrogen bond donors should be under 5 compounds.[27] Pharmacophore studies revealed that all of the compounds examined also have essential characteristics.

Furthermore, the top 10 compounds selected through molecular docking showed that all compounds showed hydrophobic interaction with mutated amino acid 533L. In Han et al. 2010 study, the complex also formed hydrophobic interactions at the wild-type amino acid F533 positions.[17] Due to the hydrophobic nature of Leucine and Phenylalanine,[28,29] wild-type and mutated amino acids showed hydrophobic interaction with compounds. Hydrophobic interactions enhance the binding affinity and stability of the drug−protein complex, making the interactions more specific and effective. Out of the 10 compounds, 8 compounds were subjected to MD simulations to gain deeper insight into the structural changes. Molecular dynamics simulations provide a dynamic perspective on the behavior of protein−ligand complexes over time. RMSD, RMSF, and Rg analyses confirm the stability of

the complex. Out of 8 compounds, 3 compounds, namely, macozinone, antibacterial agent 71, and antibacterial agent 123 showed good stability against PBP3 in RMSD analysis, which helped in understanding their dynamic behavior by providing insight into the dynamic motion of the protein−ligand complex.

The LJ-SR interaction (van der Waals) of protein−ligand complexes showed a good binding affinity. All three compounds showed a good average interaction energy with PBP3. These compounds have high interaction energies and support stable interactions with proteins. In this study, PCA analysis was used to interpret the impact of ligands and mutations on structural fluctuations. 2D projection plot analysis revealed that all three complexes occupy stable clusters. Finally, MM/GBSA analysis was used to estimate the ligand-binding affinities between the ligand and mutant PBP3. Negative binding energies for the three compounds showed a good binding affinity against the mutant PBP3.

In addition to the above study, we also analyzed the ADMET properties of hit ligands; ADMET properties are an essential feature of pharmaceutical drug design. It is frequently stated that one of the main reasons for the high attrition rates of drug candidates is the failure to achieve projected ADMET
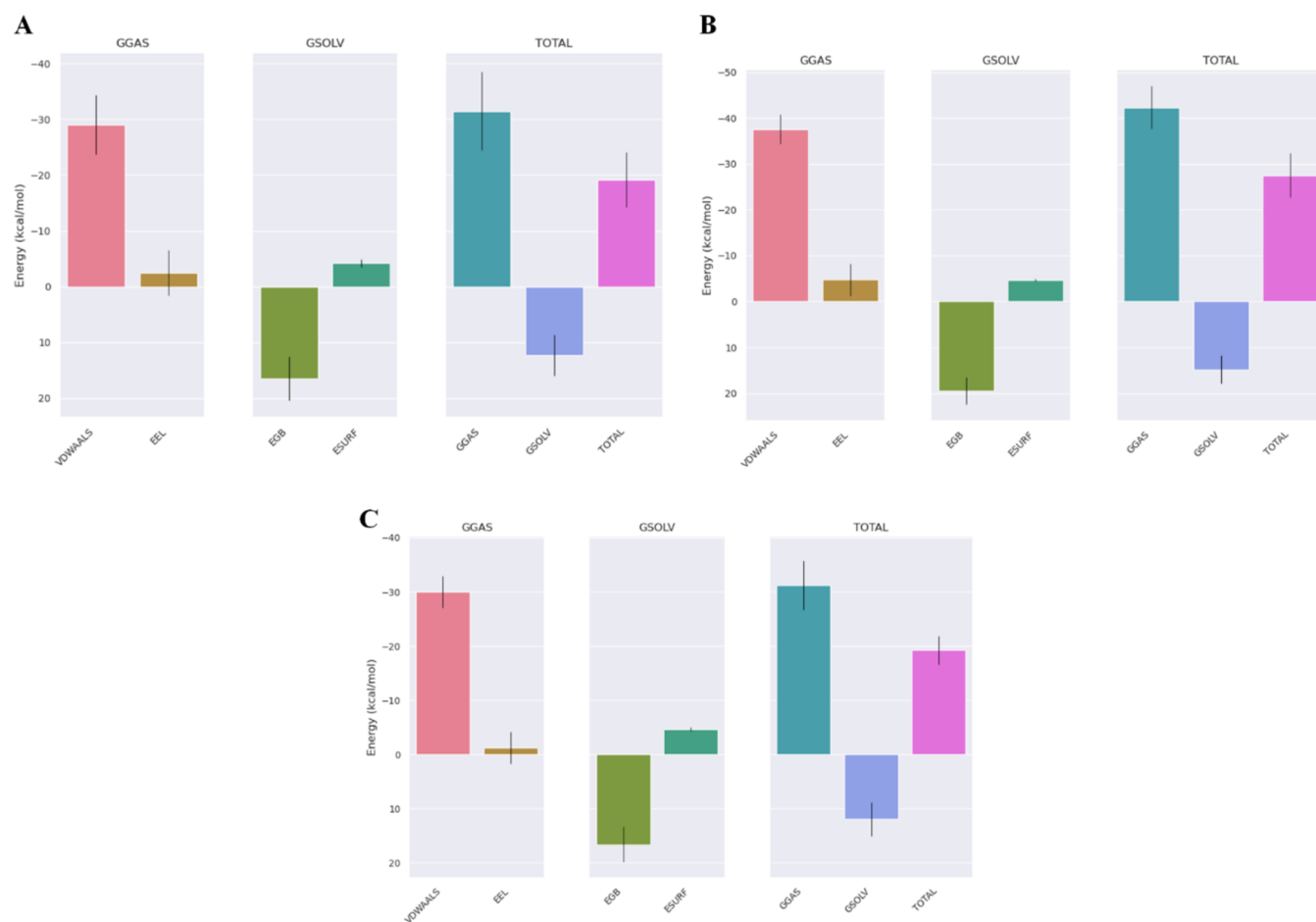
Figure 8. MMGBSA binding-free energy contribution of various interactions between the screened compounds and target proteins, i.e., (A) PBP3-macozinone, (B) PBP3-antibacterial agent 71, and (C) PBP3-antibacterial agent 123.
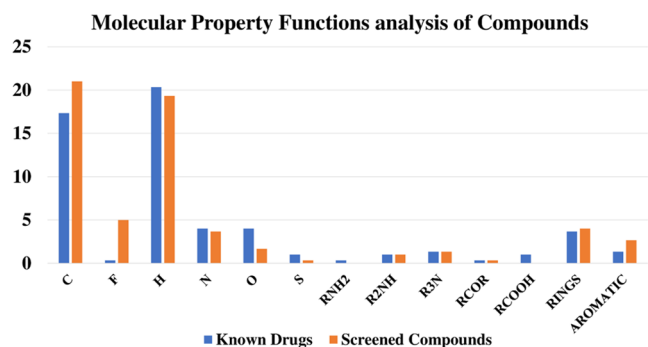
Figure 9. Molecular property functions analysis (atom counts, functional group counts, and ring counts) of known antibacterial and screened compounds.

criteria.[30] The identified hit compounds exhibit dual benefits in their noncarcinogenic nature and BBB + properties, indicating their ability to effectively penetrate the blood–brain barrier. This feature holds significant potential for therapeutic applications, particularly in the treatment of conditions that require drug delivery into the central nervous system. Additionally, analysis of HIA indicators underlines the oral administration potential of these compounds. In contemporary medicine, oral drug administration is preferred for ease of treatment and patient compliance. Determining oral bioavailability, a key factor in drug development, is inherently

challenging due to its dependence on various biological and physicochemical factors.[31] Notably, all identified hit compounds display positive characteristics related to HIA indicators, highlighting their potential as orally administered drugs with favorable bioavailability profiles.

In addition, the molecular properties of the screened compounds were analyzed and compared with known antibacterial agents, namely, cefepime, ciprofloxacin, and ampicillin. Cefepime, a broad-spectrum cephalosporin, exhibits potent activity against a diverse range of Gram-negative bacteria, including *P. aeruginosa*. Ciprofloxacin and ampicillin are also a broad-spectrum antibiotic that penetrate through the biofilm and ultimately reach distal cells.[32] Ciprofloxacin has also displayed similar penetration and proliferation activity within *P. aeruginosa* biofilms.[33] Comparison of the molecular properties of the three screened compounds, macozinone, antibacterial agent 71, and antibacterial agent 123 with known antibacterial compounds revealed similar atom counts, functional group counts, and ring counts. The presence of these molecular properties reveals their medicine-like properties.[34]

Additionally, two compounds, antibacterial agent 71 and antibacterial agent 123, are already used for research purposes. Antibacterial agent 123 is a powerful membrane-disrupting agent. Antibacterial agent 71 is also used in the research field against *Acinetobacter baumannii*, *E. coli*, and *Burkholderia cenocepacia*. Macozinone is an antituberculosis first-in-class clinical-stage benzothiazinone-based drug candidate; its efficacy and safety have been strongly proven in clinical

studies against tuberculosis.[35] All these findings against the mutated protein suggest that these compounds, mainly macozinone, antibacterial agent 71, and antibacterial agent 123, may be promising candidates for further exploration in drug development efforts.

4. CONCLUSIONS

This study focuses on identifying new compounds targeting the mutated protein of *P. aeruginosa*, specifically PBP3. PBP3 is important for bacterial growth and serves as a target for many antibiotics. Excessive use of antibiotics has led to mutations in the PBP3, including the critical 533L mutation responsible for *β*-lactam antibiotic recognition. Screening new compounds through *in-silico* methods, we analyzed protein−ligand complexes to understand the interaction with mutational point 533L. Molecular dynamics results revealed that macozinone, antibacterial agent 71, and antibacterial agent 123 displayed remarkable stability against mutant PBP3. These findings suggest their potential as novel therapeutics for addressing the challenge of antibiotic resistance in *P. aeruginosa*. Further investigation in *in vitro* studies could validate the efficacy of these compounds, providing a promising opportunity to combat antibiotic-resistant strains of *P. aeruginosa*.

5. MATERIAL AND METHODS

5.1. Mutation Analysis. PBP3 plays a vital role in the cell division of *P. aeruginosa* and serves as a well-known target for *β*-lactam antibiotics. Modifications in its structure due to mutations can greatly impact the drug efficiency, emphasizing the association of AMR. Therefore, PBP3 mutations responsible for resistance to various *β*-lactam drugs reported in the literature were collected from various scientific literature databases reported between the years 2018 and 2023.[15,23,36−45] List of all mutations of PBP3 is summarized in Supplementary Table S2.

A total of 54 mutations were reported in the functional domains of PBP3, of which 43 fell in the TP domain and remained in the dimerization domain. Among all of the mutations, 533L potentially has the greatest significance in contributing to drug resistance against *β*-lactam antibiotics because it occurred at the active site of the TP domain. Isolates carrying this mutation showed resistance to ceftolozane-tazobactam (MIC: 8/4 mg/L) along with cefepime, amoxicillin-clavulanic acid, cefotaxime, piperacillin-tazobactam, ceftazidime, aztreonam, Meropenem, and imipenem.[46] Therefore, further mutational analysis was considered only for the 533L mutation.

5.2. Protein Preparation. For the preparation of protein, with PDB ID-4KQQ,[47] the three-dimensional (3D) structure of *P. aeruginosa*'s PBP3 was obtained from the RCSB-Protein Data Bank. Furthermore, PyMOL software was used to extract all ligands, ions, and water molecules from the protein molecule. Then, utilizing the MG tools in the AutoDock Vina software, hydrogen atoms were added to the receptor molecule.[48] After preparation, the 533L mutation was structurally incorporated into the PBP3 coordinates using the mutation wizard embedded in the PyMOL 2.3.0 software.

5.3. Mutation Stability Analysis. The stability of the mutant was evaluated using two structure-based prediction servers namely DynaMut2 and DeepDDG. DynaMut2 uses normal mode analysis (NMA) and graph-based signatures to evaluate the impact of mutation on the protein's stability and dynamics.[49] DeepDDG, a neural network-based method, predicts the changes in protein's stability and functional consequence of the mutation.[50] The stability of the protein is characterized as stabilizing and destabilizing based on the $\Delta\Delta G$ value, which is the difference in the folding free energy change between the mutant and the native protein. The $\Delta\Delta G$ value below zero is defined as destabilizing, and the values above zero are defined as stabilizing mutation.

5.4. Ligand Preparation. *5.4.1. Data Collection.* Bioassay compounds with their activity against *P. aeruginosa* were obtained from PubChem (PubChem AID 566310). A total of 38 compounds (out of 38 compounds, 11 were active and 27 were inactive) were used for model construction and validation. For the test data set, a total of 274 antibacterial compounds were downloaded from PubChem. Furthermore, all compounds were screened based on 3D structure, and 127 2D compounds were omitted. Around 147 3D compounds were processed for further study.

5.4.2. Descriptor Calculation and Data Set Preprocessing. The training and testing sets of all of the compounds were uploaded in 3D-standard data (3D-SDF) format so that the PaDel program could calculate the descriptors for the compounds. A total of 1444 descriptors, including fingerprint and 2D, 3D, and 1D characteristics, were retrieved. The complete data set was examined using WEKA software before model development.[51] For the feature selection process, several WEKA functions were considered, including correlation, attribution, evaluation, and replacing missing values.[52]

5.4.3. Machine-Learning Model Prediction and Evaluation. A machine-learning model was built, using a 10-fold CV approach by implementing three different classifiers into training set compounds. To make the model accurate, three different machine-learning classifiers decision stump, decision table, and J48 were used for the training data. For a 10-fold CV, the entire set of training data is split into ten mutually exclusive subsets or folds. The predictive model's performance, which is created from the combined data of the remaining nine folds, is tested once for each fold, yielding ten different performance estimates.[53]

Each classifier's model performance was evaluated using a confusion matrix and evaluation statistics, which included further checks for specificity, sensitivity, Kappa statistic, and prediction accuracy. The following formulas were used to assess the model's accuracy

$$\text{binary classification accuracy} = \frac{TN + TP}{(TN + TP + FN + FP)}$$

$$\text{sensitivity} = \frac{TP}{(FN + TP)}$$

$$\text{specificity} = \frac{TN}{(FN + TN)}$$

kappa statistic

$$= \frac{2 \times (TP \times TN - FN \times FP)}{(FP + TP)(FP + TN) + (FN + TP)(FN + TN)}$$

TP = true positives; FP = false positives; TN = true negatives; FN = false negative.

5.5. Drug Likeness and ADMET Analysis. DruLiTo, an open-source program, was used to analyze drug likeness and

determine any potential cytotoxicity to humans. A ligand's pharmacological characteristic is determined by its bioavailability of drug likeness, which is determined by several structural and physicochemical characteristics. As a result, DruLiTo software assessed each ligand for a drug-like nature using Lipinski's five rules.[54]

ADMET are essential properties of any compound that mainly address the drug's absorption distribution, metabolism, excretion, and toxicity. ADMET properties play a vital role in the drug development time. To analyze these properties, and the biochemical and carcinogenic properties of the screened compounds, the AdmetSAR server was used.

5.6. Molecular Docking. The molecular docking analysis was carried out using PyRx, an open-source program (GUI version 0.8 of Autodock Vina), to generate a population of potential ligand orientations and conformations at the binding site.[48] The surrounding mutation site F533L in the TP domain was considered a binding site. The grid parameter of the mutated site was calculated using PyMOL 2.3.0. For the docking analysis, the center of the grid was set to $X = -5.86$, $Y = 11.89$, and $Z = 17.68$, and the grid box dimensions were set as 25 Å × 23.99 Å × 23.31 Å, and there was a difference of 0.375 Å between grid's points. The screening of all selected compounds was analyzed by rigid molecular docking into the mutation site of the PBP3. Compounds that had lower binding energies were verified and were selected for additional examination. Using the Ligplot v.1.4.5 program, the interactions of molecules between the complexes, such as the length and number of hydrogen bonds and hydrophobic bond interaction, were examined and depicted.

5.7. Molecular Dynamics (MD) Simulations. MD simulations were performed on the docked complexes by utilizing the GROMACS 2021.3[55] package. The topologies were produced using the utilization of the CHARMM 36 force field for both proteins and protein−ligand complexes.[56] Next, 12 CL ions were added to the water model to solvate all of the docked complexes and individual proteins to neutralize them. Next, energy minimization at 10 kJ/mol was carried out utilizing the Verlet cutoff strategy and the steepest descent algorithm to relax the structure. The cycle for minimizing the energy of protein and protein−ligand complex consisted of 50,000 stapes. Both NVT (constant volume) and NPT (constant pressure) were subjected to an equilibration stage over a 100 ps period. Furthermore, MD simulation was carried out at a constant temperature of 300 K and a constant pressure of 1 atm using a time step of 2 fs for a 100 ns time scale. The behavior of each complex was examined by using the generated trajectories to see whether the system was stable in the explicit water environment. RMSD, RMSF, Rg, hydrogen bonds, the LJ-SR interaction (van der Waals) energy, and PCA were used to examine the deviations of the protein and protein−ligand complex system.

Subsequently, the protein−ligand complex MD simulation findings were validated using the generalized Born and surface area solvation (MM/GBSA) technique, which is integrated into the g_mmpbsa program.[57,58] For three protein−ligand complexes, the ΔG_{TOTAL} binding-free energy was found using the MD simulation trajectory. The system's temperature was set to 298.15 and the solvation parameter (igb) to 5. For other parameters, such as the internal and exterior dielectric constants, which are 1.0 and 78.5, respectively, the default values were applied.

5.8. Molecular Property Functions Analysis of Compounds. The molecular properties such as atom counts, functional group counts, and ring counts of known antibacterial compounds and screened compounds were analyzed by R software (version 3.4.3) under the library of "ChemmineR".[59]

■ ASSOCIATED CONTENT

Data Availability Statement

All of the data has been included in the Supporting Information and has been attached to the manuscript.

ⓢ Supporting Information

The Supporting Information is available free of charge at https://pubs.acs.org/doi/10.1021/acsomega.4c00929.

(Table S1) drug likeness properties of all screened compounds and (Table S2) list of mutations of PBP3 in *P. aeruginosa* collected from literatures (PDF)

■ AUTHOR INFORMATION

Corresponding Authors

Sudha Ramaiah − *Medical and Biological Computing Laboratory, School of Biosciences and Technology, Vellore Institute of Technology (VIT), Vellore 632014 Tamil Nadu, India; Department of Bio-Sciences, School of Biosciences and Technology, Vellore Institute of Technology (VIT), Vellore 632014 Tamil Nadu,, India;* ⓞ orcid.org/0000-0002-4800-329X; Phone: +91-416-2556/2694; Email: sudhaanand@vit.ac.in; Fax: +91-416 2243092

Anand Anbarasu − *Medical and Biological Computing Laboratory, School of Biosciences and Technology, Vellore Institute of Technology (VIT), Vellore 632014 Tamil Nadu, India; Department of Biotechnology, School of Biosciences and Technology, Vellore Institute of Technology (VIT), Vellore 632014 Tamil Nadu, India;* ⓞ orcid.org/0000-0003-2216-7488; Phone: +91-416-2556/2694; Email: aanand@vit.ac.in; Fax: +91-416-2243092

Authors

Tushar Joshi − *Medical and Biological Computing Laboratory, School of Biosciences and Technology, Vellore Institute of Technology (VIT), Vellore 632014 Tamil Nadu, India; Department of Biotechnology, School of Biosciences and Technology, Vellore Institute of Technology (VIT), Vellore 632014 Tamil Nadu, India*

Santhiya Vijayakumar − *Medical and Biological Computing Laboratory, School of Biosciences and Technology, Vellore Institute of Technology (VIT), Vellore 632014 Tamil Nadu, India; Department of Integrative Biology, School of Biosciences and Technology (SBST), Vellore Institute of Technology (VIT), Vellore 632014, India*

Soumyadip Ghosh − *Medical and Biological Computing Laboratory, School of Biosciences and Technology, Vellore Institute of Technology (VIT), Vellore 632014 Tamil Nadu, India; Department of Bio-Sciences, School of Biosciences and Technology, Vellore Institute of Technology (VIT), Vellore 632014 Tamil Nadu,, India*

Shalini Mathpal − *Medical and Biological Computing Laboratory, School of Biosciences and Technology, Vellore Institute of Technology (VIT), Vellore 632014 Tamil Nadu, India; Department of Bio-Sciences, School of Biosciences and Technology, Vellore Institute of Technology (VIT), Vellore 632014 Tamil Nadu,, India*

Complete contact information is available at:
https://pubs.acs.org/10.1021/acsomega.4c00929

Author Contributions
⊥T.J. and S.V. have contributed equally. T.J. and S.V.: conceptualization, methodology, writing the original article, and editing; T.J. and S.G.: formal analysis and validation; T.J. and S.M.: figure preparation; A.A. and S.R: investigation, visualization, reviewing, supervision, and funding.

Notes
The authors declare no competing financial interest.

■ REFERENCES
(1) Lyczak, J. B.; Cannon, C. L.; Pier, G. B. Establishment of Infection: Lessons from a Versatile Opportunist. *Microbes Infect.* **2000**, *2* (9), 1051−1060.

(2) Talebi, M.; Minai-Tehrani, D.; Fazilati, M.; Minai-Tehrani, A. Inhibitory Action of Dicyclomine on Lipase Activity, Kinetics and Molecular Study. *Int. J. Biol. Macromol.* **2018**, *107*, 2422−2428.

(3) Flockton, T.; Schnorbus, L.; Araujo, A.; Adams, J.; Hammel, M.; Perez, L. Inhibition of Pseudomonas Aeruginosa Biofilm Formation with Surface Modified Polymeric Nanoparticles. *Pathogens* **2019**, *8* (2), 55.

(4) Gellatly, S. L.; Hancock, R. E. W. Pseudomonas Aeruginosa: New Insights into Pathogenesis and Host Defenses. *Pathog. Dis.* **2013**, *67* (3), 159−173.

(5) Bassetti, M.; Vena, A.; Croxatto, A.; Righi, E.; Guery, B. How to Manage Pseudomonas Aeruginosa Infections. *Drugs Context* **2018**, *7*, 1−18.

(6) Laborda, P.; Sanz-García, F.; Hernando-Amado, S.; Martínez, J. L. Pseudomonas Aeruginosa: An Antibiotic Resilient Pathogen with Environmental Origin. *Curr. Opin. Microbiol.* **2021**, *64*, 125−132.

(7) Reynolds, D.; Kollef, M. The Epidemiology and Pathogenesis and Treatment of Pseudomonas Aeruginosa Infections: An Update. *Drugs* **2021**, *81* (18), 2117−2131.

(8) Asokan, G.; Ramadhan, T.; Ahmed, E.; Sanad, H. WHO Global Priority Pathogens List: A Bibliometric Analysis of Medline-PubMed for Knowledge Mobilization to Infection Prevention and Control Practices in Bahrain. *Oman Med. J.* **2019**, *34* (3), 184−193.

(9) López-de-la-Cruz, J.; Pérez-Aranda, M.; Alcudia, A.; Begines, B.; Caraballo, T.; Pajuelo, E.; Ginel, P. J. Dynamics and Numerical Simulations to Predict Empirical Antibiotic Treatment of Multi-Resistant Pseudomonas Aeruginosa Infection. *Commun. Nonlinear Sci. Numer. Simul.* **2020**, *91*, No. 105418.

(10) Murray, C. J. L.; Ikuta, K. S.; Sharara, F.; Swetschinski, L.; Robles Aguilar, G.; Gray, A.; Han, C.; Bisignano, C.; Rao, P.; Wool, E.; Johnson, S. C.; Browne, A. J.; Chipeta, M. G.; Fell, F.; Hackett, S.; Haines-Woodhouse, G.; Kashef Hamadani, B. H.; Kumaran, E. A. P.; McManigal, B.; Achalapong, S.; Agarwal, R.; Akech, S.; Albertson, S.; Amuasi, J.; Andrews, J.; Aravkin, A.; Ashley, E.; Babin, F.-X.; Bailey, F.; Baker, S.; Basnyat, B.; Bekker, A.; Bender, R.; Berkley, J. A.; Bethou, A.; Bielicki, J.; Boonkasidecha, S.; Bukosia, J.; Carvalheiro, C.; Castañeda-Orjuela, C.; Chansamouth, V.; Chaurasia, S.; Chiurchiù, S.; Chowdhury, F.; Clotaire Donatien, R.; Cook, A. J.; Cooper, B.; Cressey, T. R.; Criollo-Mora, E.; Cunningham, M.; Darboe, S.; Day, N. P. J.; De Luca, M.; Dokova, K.; Dramowski, A.; Dunachie, S. J.; Duong Bich, T.; Eckmanns, T.; Eibach, D.; Emami, A.; Feasey, N.; Fisher-Pearson, N.; Forrest, K.; Garcia, C.; Garrett, D.; Gastmeier, P.; Giref, A. Z.; Greer, R. C.; Gupta, V.; Haller, S.; Haselbeck, A.; Hay, S. I.; Holm, M.; Hopkins, S.; Hsia, Y.; Iregbu, K. C.; Jacobs, J.; Jarovsky, D.; Javanmardi, F.; Jenney, A. W. J.; Khorana, M.; Khusuwan, S.; Kissoon, N.; Kobeissi, E.; Kostyanev, T.; Krapp, F.; Krumkamp, R.; Kumar, A.; Kyu, H. H.; Lim, C.; Lim, K.; Limmathurotsakul, D.; Loftus, M. J.; Lunn, M.; Ma, J.; Manoharan, A.; Marks, F.; May, J.; Mayxay, M.; Mturi, N.; Munera-Huertas, T.; Musicha, P.; Musila, L. A.; Mussi-Pinhata, M. M.; Naidu, R. N.; Nakamura, T.; Nanavati, R.; Nangia, S.; Newton, P.; Ngoun, C.; Novotney, A.; Nwakanma, D.; Obiero, C. W.; Ochoa, T. J.; Olivas-Martinez, A.; Olliaro, P.; Ooko, E.; Ortiz-Brizuela, E.; Ounchanum, P.; Pak, G. D.; Paredes, J. L.; Peleg, A. Y.; Perrone, C.; Phe, T.; Phommasone, K.; Plakkal, N.; Ponce-de-Leon, A.; Raad, M.; Ramdin, T.; Rattanavong, S.; Riddell, A.; Roberts, T.; Robotham, J. V.; Roca, A.; Rosenthal, V. D.; Rudd, K. E.; Russell, N.; Sader, H. S.; Saengchan, W.; Schnall, J.; Scott, J. A. G.; Seekaew, S.; Sharland, M.; Shivamallappa, M.; Sifuentes-Osornio, J.; Simpson, A. J.; Steenkeste, N.; Stewardson, A. J.; Stoeva, T.; Tasak, N.; Thaiprakong, A.; Thwaites, G.; Tigoi, C.; Turner, C.; Turner, P.; van Doorn, H. R.; Velaphi, S.; Vongpradith, A.; Vongsouvath, M.; Vu, H.; Walsh, T.; Walson, J. L.; Waner, S.; Wangrangsimakul, T.; Wannapinij, P.; Wozniak, T.; Young Sharma, T. E. M. W.; Yu, K. C.; Zheng, P.; Sartorius, B.; Lopez, A. D.; Stergachis, A.; Moore, C.; Dolecek, C.; Naghavi, M. Global Burden of Bacterial Antimicrobial Resistance in 2019: A Systematic Analysis. *Lancet* **2022**, *399* (10325), 629−655.

(11) Brindhadevi, K.; LewisOscar, F.; Mylonakis, E.; Shanmugam, S.; Verma, T. N.; Pugazhendhi, A. Biofilm and Quorum Sensing Mediated Pathogenicity in Pseudomonas Aeruginosa. *Process Biochem.* **2020**, *96*, 49−57.

(12) Qin, S.; Xiao, W.; Zhou, C.; Pu, Q.; Deng, X.; Lan, L.; Liang, H.; Song, X.; Wu, M. Pseudomonas Aeruginosa: Pathogenesis, Virulence Factors, Antibiotic Resistance, Interaction with Host, Technology Advances and Emerging Therapeutics. *Signal Transduct. Target. Ther.* **2022**, *7* (1), 199.

(13) Glen, K. A.; Lamont, I. L. β-Lactam Resistance in Pseudomonas Aeruginosa: Current Status, Future Prospects. *Pathogens* **2021**, *10* (12), 1638.

(14) López-Pérez, A.; Freischem, S.; Grimm, I.; Weiergräber, O.; Dingley, A.; López-Alberca, M.; Waldmann, H.; Vollmer, W.; Kumar, K.; Vuong, C. Discovery of Pyrrolidine-2,3-Diones as Novel Inhibitors of P. Aeruginosa PBP3. *Antibiotics* **2021**, *10* (5), 529.

(15) Cabot, G.; Zamorano, L.; Moyà, B.; Juan, C.; Navas, A.; Blázquez, J.; Oliver, A. Evolution of Pseudomonas Aeruginosa Antimicrobial Resistance and Fitness under Low and High Mutation Rates. *Antimicrob. Agents Chemother.* **2016**, *60* (3), 1767−1778.

(16) Oliver, A.; Rojo-Molinero, E.; Arca-Suarez, J.; Beşli, Y.; Bogaerts, P.; Cantón, R.; Cimen, C.; Croughs, P. D.; Denis, O.; Giske, C. G.; Graells, T.; Daniel Huang, T.-D.; Iorga, B. I.; Karatuna, O.; Kocsis, B.; Kronenberg, A.; López-Causapé, C.; Malhotra-Kumar, S.; Martínez, L. M.; Mazzariol, A.; Meyer, S.; Naas, T.; Notermans, D. W.; Oteo-Iglesias, J.; Pedersen, T.; Pirš, M.; Poeta, P.; Poirel, L.; Pournaras, S.; Sundsfjord, A.; Szabó, D.; Tambić-Andrašević, A.; Vatcheva-Dobrevska, R.; Vitkauskienė, A.; Jeannot, K. Pseudomonas Aeruginosa Antimicrobial Susceptibility Profiles, Resistance Mechanisms and International Clonal Lineages: Update from ESGARS-ESCMID/ISARPAE Group. *Clin. Microbiol. Infect.* **2024**, *30*, 469 DOI: 10.1016/j.cmi.2023.12.026.

(17) Han, S.; Zaniewski, R. P.; Marr, E. S.; Lacey, B. M.; Tomaras, A. P.; Evdokimov, A.; Miller, J. R.; Shanmugasundaram, V. Structural Basis for Effectiveness of Siderophore-Conjugated Monocarbams against Clinically Relevant Strains of Pseudomonas Aeruginosa. *Proc. Natl. Acad. Sci. U. S. A.* **2010**, *107* (51), 22002−22007.

(18) Meletis, G. Carbapenem Resistance: Overview of the Problem and Future Perspectives. *Ther. Adv. Infect. Dis.* **2016**, *3* (1), 15−21.

(19) Diaz Caballero, J.; Clark, S. T.; Coburn, B.; Zhang, Y.; Wang, P. W.; Donaldson, S. L.; Tullis, D. E.; Yau, Y. C. W.; Waters, V. J.; Hwang, D. M.; Guttman, D. S. Selective Sweeps and Parallel Pathoadaptation Drive Pseudomonas Aeruginosa Evolution in the Cystic Fibrosis Lung. *mBio* **2015**, *6* (5), e00981-15 DOI: 10.1128/mBio.00981-15.

(20) López-Causapé, C.; Sommer, L. M.; Cabot, G.; Rubio, R.; Ocampo-Sosa, A. A.; Johansen, H. K.; Figuerola, J.; Cantón, R.; Kidd, T. J.; Molin, S.; Oliver, A. Evolution of the Pseudomonas Aeruginosa Mutational Resistome in an International Cystic Fibrosis Clone. *Sci. Rep.* **2017**, *7* (1), No. 5555.

(21) Jorth, P.; McLean, K.; Ratjen, A.; Secor, P. R.; Bautista, G. E.; Ravishankar, S.; Rezayat, A.; Garudathri, J.; Harrison, J. J.; Harwood, R. A.; Penewit, K.; Waalkes, A.; Singh, P. K.; Salipante, S. J. Evolved Aztreonam Resistance Is Multifactorial and Can Produce Hypervirulence in Pseudomonas Aeruginosa. *mBio* **2017**, *8* (5), e00517-17 DOI: 10.1128/mBio.00517-17.

(22) Cabot, G.; Florit-Mendoza, L.; Sánchez-Diener, I.; Zamorano, L.; Oliver, A. Deciphering β-Lactamase-Independent β-Lactam Resistance Evolution Trajectories in Pseudomonas Aeruginosa. *J. Antimicrob. Chemother.* **2018**, *73* (12), 3322−3331.

(23) Clark, S. T.; Sinha, U.; Zhang, Y.; Wang, P. W.; Donaldson, S. L.; Coburn, B.; Waters, V. J.; Yau, Y. C. W.; Tullis, D. E.; Guttman, D. S.; Hwang, D. M. Penicillin-Binding Protein 3 Is a Common Adaptive Target among Pseudomonas Aeruginosa Isolates from Adult Cystic Fibrosis Patients Treated with β-Lactams. *Int. J. Antimicrob. Agents* **2019**, *53* (5), 620−628.

(24) Sahare, P.; Moon, A. IN-SILICO Docking Studies of Phytoligands Against *E. COLI* PBP3: Approach Towards Novel Antibacterial Therapeutic Agent Maharashtra, India. *Int. J. Pharm. Sci. Res.* **2016**, *7* (9), 3703−3711.

(25) Kumar, H.; Manoharan, A.; Ramaiah, S. Unravelling the NsSNP Mediated Mechanism of Antibiotic Resistance in Salmonella Enterica Serovar Typhi and Identification of Potential Therapeutic Alternatives: A Genomics and Structural Bioinformatics Study. *Clin. Epidemiol. Glob. Heal.* **2023**, *24*, No. 101407.

(26) Sauvage, E.; Terrak, M. Glycosyltransferases and Transpeptidases/Penicillin-Binding Proteins: Valuable Targets for New Antibacterials. *Antibiotics* **2016**, *5* (1), 12.

(27) Lipinski, C. A. Lead- and Drug-like Compounds: The Rule-of-Five Revolution. *Drug Discovery Today Technol.* **2004**, *1* (4), 337−341.

(28) AL Mughram, M. H.; Catalano, C.; Herrington, N. B.; Safo, M. K.; Kellogg, G. E. 3D Interaction Homology: The Hydrophobic Residues Alanine, Isoleucine, Leucine, Proline and Valine Play Different Structural Roles in Soluble and Membrane Proteins. *Front. Mol. Biosci.* **2023**, *10*, 1116868 DOI: 10.3389/fmolb.2023.1116868.

(29) Widyarani; Sari, Y. W.; Ratnaningsih, E.; Sanders, J. P. M.; Bruins, M. E. Production of Hydrophobic Amino Acids from Biobased Resources: Wheat Gluten and Rubber Seed Proteins. *Appl. Microbiol. Biotechnol.* **2016**, *100* (18), 7909−7920.

(30) Ferreira, L. L. G.; Andricopulo, A. D. ADMET Modeling Approaches in Drug Discovery. *Drug Discovery Today* **2019**, *24* (5), 1157−1165.

(31) Hou, T.; Wang, J.; Li, Y. ADME Evaluation in Drug Discovery. 8. The Prediction of Human Intestinal Absorption by a Support Vector Machine. *J. Chem. Inf. Model.* **2007**, *47* (6), 2408−2415.

(32) Anderl, J. N.; Franklin, M. J.; Stewart, P. S. Role of Antibiotic Penetration Limitation in Klebsiella Pneumoniae Biofilm Resistance to Ampicillin and Ciprofloxacin. *Antimicrob. Agents Chemother.* **2000**, *44* (7), 1818−1824.

(33) Walters, M. C.; Roe, F.; Bugnicourt, A.; Franklin, M. J.; Stewart, P. S. Contributions of Antibiotic Penetration, Oxygen Limitation, and Low Metabolic Activity to Tolerance of Pseudomonas Aeruginosa Biofilms to Ciprofloxacin and Tobramycin. *Antimicrob. Agents Chemother.* **2003**, *47* (1), 317−323.

(34) Nand, M.; Maiti, P.; Joshi, T.; Chandra, S.; Pande, V.; Kuniyal, J. C.; Ramakrishnan, M. A. Virtual Screening of Anti-HIV1 Compounds against SARS-CoV-2: Machine Learning Modeling, Chemoinformatics and Molecular Dynamics Simulation Based Analysis. *Sci. Rep.* **2020**, *10* (1), No. 20397.

(35) Mariandyshev, A. O.; Khokhlov, A. L.; Smerdin, S. V.; Shcherbakova, V. S.; Igumnova, O. V.; Ozerova, I. V.; Bolgarina, A. A.; Nikitina, N. A. The Main Results of Clinical Trials of the Efficacy, Safety and Pharmacokinetics of the Perspective Anti-Tuberculosis Drug Makozinone (PBTZ169). *Ter. Arkh.* **2020**, *92* (3), 61−72.

(36) Barceló, I.; Cabot, G.; Palwe, S.; Joshi, P.; Takalkar, S.; Periasamy, H.; Cortés-Lara, S.; Zamorano, L.; Sánchez-Diener, I.; Moya, B.; Bhagwat, S.; Patel, M.; Oliver, A. In Vitro Evolution of Cefepime/Zidebactam (WCK 5222) Resistance in Pseudomonas Aeruginosa: Dynamics, Mechanisms, Fitness Trade-off and Impact on in Vivo Efficacy. *J. Antimicrob. Chemother.* **2021**, *76* (10), 2546−2557.

(37) López-Causapé, C.; Rubio, R.; Cabot, G.; Oliver, A. Evolution of the Pseudomonas Aeruginosa Aminoglycoside Mutational Resistome In Vitro and in the Cystic Fibrosis Setting. *Antimicrob. Agents Chemother.* **2018**, *62* (4), e02583-17 DOI: 10.1128/AAC.02583-17.

(38) Mojica, M. F.; De La Cadena, E.; García-Betancur, J. C.; Porras, J.; Novoa-Caicedo, I.; Páez-Zamora, L.; Pallares, C.; Appel, T. M.; Radice, M. A.; Castañeda-Méndez, P.; Gales, A. C.; Munita, J. M.; Villegas, M. V. Molecular Mechanisms of Resistance to Ceftazidime/Avibactam in Clinical Isolates of Enterobacterales and Pseudomonas Aeruginosa in Latin American Hospitals. *mSphere* **2023**, *8* (2), e0065122 DOI: 10.1128/msphere.00651-22.

(39) Gaibani, P.; Giani, T.; Bovo, F.; Lombardo, D.; Amadesi, S.; Lazzarotto, T.; Coppi, M.; Rossolini, G. M.; Ambretti, S. Resistance to Ceftazidime/Avibactam, Meropenem/Vaborbactam and Imipenem/Relebactam in Gram-Negative MDR Bacilli: Molecular Mechanisms and Susceptibility Testing. *Antibiotics* **2022**, *11* (5), 628.

(40) Bellini, D.; Koekemoer, L.; Newman, H.; Dowson, C. G. Novel and Improved Crystal Structures of H. Influenzae, *E. Coli* and P. Aeruginosa Penicillin-Binding Protein 3 (PBP3) and N. Gonorrhoeae PBP2: Toward a Better Understanding of β-Lactam Target-Mediated Resistance. *J. Mol. Biol.* **2019**, *431* (18), 3501−3519.

(41) Colque, C. A.; Albarracín Orio, A. G.; Feliziani, S.; Marvig, R. L.; Tobares, A. R.; Johansen, H. K.; Molin, S.; Smania, A. M. Hypermutator Pseudomonas Aeruginosa Exploits Multiple Genetic Pathways To Develop Multidrug Resistance during Long-Term Infections in the Airways of Cystic Fibrosis Patients. *Antimicrob. Agents Chemother.* **2020**, *64* (5), e02142-19 DOI: 10.1128/AAC.02142-19.

(42) del Barrio-Tofiño, E.; Zamorano, L.; Cortes-Lara, S.; López-Causapé, C.; Sánchez-Diener, I.; Cabot, G.; Bou, G.; Martínez-Martínez, L.; Oliver, A.; Group, G.-S. P. study; Galán, F.; Gracia, I.; Rodríguez, M. A.; Martín, L.; Sánchez, J. M.; Viñuela, L.; García, M. V.; Lepe, J. A.; Aznar, J.; López-Hernández, I.; Seral, C.; Javier Castillo-García, F.; López-Calleja, A. I.; Aspiroz, C.; de la Iglesia, P.; Ramón, S.; Riera, E.; Cruz Pérez, M.; Gallegos, C.; Calvo, J.; Dolores Quesada, M.; Marco, F.; Hoyos, Y.; Pablo Horcajada, J.; Larrosa, N.; González, J. J.; Tubau, F.; Capilla, S.; Pérez-Moreno, M. O.; Centelles, M. J.; Padilla, E.; Rivera, A.; Mirelis, B.; Elisa Rodríguez-Tarazona, R.; Arenal-Andrés, N.; del Pilar Ortega, M.; Megías, G.; García, I.; Colmenarejo, C.; González, J. C.; Martínez, N. M.; Gomila, B.; Giner, S.; Tormo, N.; Garduño, E.; Agulla, J. A.; Seoane, A.; Pita, J.; Vidal, I. P.; Guzmán, D. M.; García, M.; Pérez del Molino, M. L.; Barbeito, G.; Artiles, F.; Azcona-Gutiérrez, J. M.; Sáenz, Y.; Antonio Oteo, J.; González, A.; Villa, J.; Chaves, F.; Cercenado, E.; Alarcón, T.; Zurita, N. D.; Merino, I.; Morosini, M. I.; Cantón, R.; Isabel Sánchez, M.; Moreno, L.; Yagüe, G.; Leiva, J.; Luis Barrios, J.; Canut, A.; Oteo, J. Spanish Nationwide Survey on Pseudomonas Aeruginosa Antimicrobial Resistance Mechanisms and Epidemiology. *J. Antimicrob. Chemother.* **2019**, *74* (7), 1825−1835.

(43) McLean, K.; Lee, D.; Holmes, E. A.; Penewit, K.; Waalkes, A.; Ren, M.; Lee, S. A.; Gasper, J.; Manoil, C.; Salipante, S. J. Genomic Analysis Identifies Novel Pseudomonas Aeruginosa Resistance Genes under Selection during Inhaled Aztreonam Therapy In Vivo. *Antimicrob. Agents Chemother.* **2019**, *63* (9), e00866-19 DOI: 10.1128/AAC.00866-19.

(44) Tueffers, L.; Barbosa, C.; Bobis, I.; Schubert, S.; Höppner, M.; Rühlemann, M.; Franke, A.; Rosenstiel, P.; Friedrichs, A.; Krenz-Weinreich, A.; Fickenscher, H.; Bewig, B.; Schreiber, S.; Schulenburg, H. Pseudomonas Aeruginosa Populations in the Cystic Fibrosis Lung Lose Susceptibility to Newly Applied β-Lactams within 3 Days. *J. Antimicrob. Chemother.* **2019**, *74* (10), 2916−2925.

(45) Gomis-Font, M. A.; Cabot, G.; Sánchez-Diener, I.; Fraile-Ribot, P. A.; Juan, C.; Moya, B.; Zamorano, L.; Oliver, A. In Vitro Dynamics and Mechanisms of Resistance Development to Imipenem and Imipenem/Relebactam in Pseudomonas Aeruginosa. *J. Antimicrob. Chemother.* **2020**, *75* (9), 2508−2515.

(46) Hernández-García, M.; Sánchez-López, J.; Martínez-García, L.; Becerra-Aparicio, F.; Morosini, M. I.; Ruiz-Garbajosa, P.; Cantón, R. Emergence of the New KPC-49 Variant Conferring an ESBL Phenotype with Resistance to Ceftazidime-Avibactam in the ST131-H30R1 *Escherichia Coli* High-Risk Clone. *Pathogens* **2021**, *10* (1), 67.

(47) van Berkel, S. S.; Nettleship, J. E.; Leung, I. K. H.; Brem, J.; Choi, H.; Stuart, D. I.; Claridge, T. D. W.; McDonough, M. A.; Owens, R. J.; Ren, J.; Schofield, C. J. Binding of (5 S)-Penicilloic Acid to Penicillin Binding Protein 3. *ACS Chem. Biol.* **2013**, *8* (10), 2112−2116.

(48) Trott, O.; Olson, A. J. Autodock Vina: Improving the Speed and Accuracy of Docking. *J. Comput. Chem.* **2010**, *31* (2), 455−461.

(49) Rodrigues, C. H. M.; Pires, D. E. V.; Ascher, D. B. <scp > DynaMut2</Scp>: Assessing Changes in Stability and Flexibility upon Single and Multiple Point Missense Mutations. *Protein Sci.* **2021**, *30* (1), 60−69.

(50) Cao, H.; Wang, J.; He, L.; Qi, Y.; Zhang, J. Z. DeepDDG: Predicting the Stability Change of Protein Point Mutations Using Neural Networks. *J. Chem. Inf. Model.* **2019**, *59* (4), 1508−1514.

(51) Asha Kiranmai, S.; Jaya Laxmi, A. Data Mining for Classification of Power Quality Problems Using WEKA and the Effect of Attributes on Classification Accuracy. *Prot. Control Mod. Power Syst.* **2018**, *3* (1), 29.

(52) Nand, M.; Maiti, P.; Joshi, T.; Chandra, S.; Pande, V.; Kuniyal, J. C.; Ramakrishnan, M. A. Virtual Screening of Anti-HIV1 Compounds against SARS-CoV-2: Machine Learning Modeling, Chemoinformatics and Molecular Dynamics Simulation Based Analysis. *Sci. Rep.* **2020**, *10* (1), No. 20397.

(53) Kohavi, R. A Study of Cross-Validation and Bootstrap for Accuracy Estimation and Model Selection. In *Proc. 14th Int. Conf. AI*; Morgan Kaufmann: San Mateo, CA, 1995; pp 1137−1145.

(54) Leeson, P. Drug Discovery: Chemical Beauty Contest. *Nature* **2012**, *481* (7382), 455−456.

(55) Lindahl; Abraham; Hess; DerSpoel, V. *V. GROMACS 2021.3 Manual (2021.3)*, Zenodo, 2021 https://doi.org/https://doi.org/10.5281/zenodo.5053220.

(56) Vanommeslaeghe, K.; Hatcher, E.; Acharya, C.; Kundu, S.; Zhong, S.; Shim, J.; Darian, E.; Guvench, O.; Lopes, P.; Vorobyov, I.; Mackerell, A. D. CHARMM General Force Field: A Force Field for Drug-like Molecules Compatible with the CHARMM All-Atom Additive Biological Force Fields. *J. Comput. Chem.* **2010**, *31*, 671−690.

(57) Miller, B. R.; McGee, T. D.; Swails, J. M.; Homeyer, N.; Gohlke, H.; Roitberg, A. E. MMPBSA.Py: An Efficient Program for End-State Free Energy Calculations. *J. Chem. Theory Comput.* **2012**, *8* (9), 3314−3321.

(58) Valdés-Tresanco, M. S.; Valdés-Tresanco, M. E.; Valiente, P. A.; Moreno, E. Gmx_MMPBSA: A New Tool to Perform End-State Free Energy Calculations with GROMACS. *J. Chem. Theory Comput.* **2021**, *17* (10), 6281−6291.

(59) Cao, Y.; Charisi, A.; Cheng, L. C.; Jiang, T.; Girke, T. ChemmineR: A Compound Mining Framework for R. *Bioinformatics* **2008**, *24*, 1733−1734.